Computer simulation of the ground-state atomic configurations of Ni-Al clusters using the embedded-atom model

C. Rey, J. García-Rodeja, and L. J. Gallego
Departamento de Física de la Materia Condensada, Facultad de Física, Universidad de Santiago de Compostela, Santiago de Compostela, E-15706 Spain
(Received 6 December 1995; revised manuscript received 22 February 1996)

Using the Voter and Chen version of the embedded-atom model, we performed molecular-dynamics simulations to determine the ground-state atomic configurations of $Ni_{n-x}Al_x$ clusters ($n=13$, 19, and 55) for all concentrations x. The lowest-energy structures of both the bimetallic and the pure ($x=0$ and n) clusters are icosahedral. In general, there is a tendency for Al atoms to be segregated at the surfaces of the bimetallic clusters, although this effect can coexist with ordering. However, in the large $Ni_{54}Al$ cluster the Al impurity is located at the 12-coordinate central site, i.e., ordering predominates over segregation.
[S0163-1829(96)11327-8]

I. INTRODUCTION

Provided that the model interaction potentials used are accurate enough, computer simulation methods can allow a reliable description of the structural and dynamic properties of small clusters. The systems that have been studied in this way include Lennard-Jones, ionic, covalent and metallic clusters (see, e.g., Ref. 1 and references cited therein). However, work in this area has primarily focused on systems containing only one species of atom, although a small number of simulation studies of Lennard-Jones[2–4] or metallic[5–7] binary clusters have also been carried out, and have thrown light on the ordering and segregation tendencies in this kind of system. The study of bimetallic clusters, in which many-body effects are significant, is particularly interesting for both theoretical and technological reasons: bimetallic clusters are used as catalysts in the automobile industry and in oil refining,[8,9] and since the reactions catalyzed occur at the cluster surface it is of prime importance to know which component will tend to occupy the surface sites.

Recently, Montejano-Carrizales, Iñiguez, and Alonso[10] have used the Foiles, Baskes, and Daw[11] (FBD) version of the embedded-atom model (EAM) to investigate ordering and segregation in 55- and 147-atom Cu-Ni and Cu-Pd clusters. However, in spite of the usefulness of this approach for interpreting the surface and bulk properties of transition metals,[11] its reliability for a description of the peculiar features of small metal clusters can be questioned. As was shown in Ref. 1, both the FBD EAM and the tight-binding method (TBM) (Refs. 12 and 13) often fail to reproduce the enhanced stability of icosahedral 13- and 19-atom transition-metal clusters, predicting binding energies which deviate from the values obtained by *ab initio* calculations in the cases in which such values are available.[14] Moreover, Montejano-Carrizales, Iñiguez, and Alonso only considered ideal icosahedral and cuboctahedral clusters with fixed interatomic distances, a restriction which must be eliminated in a more general investigation of the structural behavior of bimetallic clusters.

In Ref. 15 we showed that a more accurate description of the properties of one-component clusters of fcc transition metals can be provided, within the context of the EAM, by using the version proposed by Voter and Chen,[16] which differs from that of Foiles, Baskes, and Daw in two main ways: (a) its core-core pair interaction has a medium-range attractive contribution (rather than being entirely repulsive); and (b) properties of the diatomic molecule were used in fitting the embedding function and pair interaction. In view of those results, the question arises whether the Voter and Chen version of the EAM, in the form in which this model is applied to binary alloys,[16] also allows a reliable description of the characteristic features of bimetallic clusters.

This paper describes an extensive molecular-dynamics MD study of the ground-state structures and ordering tendencies of $Ni_{n-x}Al_x$ clusters ($n=13$, 19, and 55; $0\leqslant x\leqslant n$) at low temperature. The choice of this kind of heterocluster was not arbitrary: the considerable amount of experimental data on Ni-Al alloys allows the construction of an optimized interatomic potential for this system. In particular, Voter and Chen[16] have derived an EAM potential that is capable of describing pure Ni (fcc), pure Al (fcc), diatomic Ni_2, diatomic Al_2, Ni_3Al ($L1_2$), and NiAl ($B2$), and it is reasonable to hope that this potential may also give a satisfactory description of the properties of Ni-Al clusters. There have also been theoretical studies of this kind of bimetallic cluster, the results of which may be compared with those of our work: Gong and Kumar[17] have used density-functional theory, with the local-spin-density approximation, to calculate the relative stabilities of icosahedral $Al_{12}M$ clusters in which the transition-metal M atom lies at the center of the icosahedron. Gong and Kumar's results predict that such clusters will be highly stable when M is from the middle of a d series, which provides insight into the formation of Al-M quasicrystals for certain M. For the particular case of $Al_{12}Ni$, Gong and Kumar found significantly stronger binding than in the pure Al_{13} cluster, a result which, as will be seen, agrees with our EAM-based MD findings.

This paper is organized as follows. In Sec. II we briefly describe the Voter and Chen EAM potential for the binary Ni-Al system, and specify certain technical details of the MD simulations used in this work to determine ground-state clus-

ter structures. In Sec. III we present and discuss our results, and in Sec. IV we summarize our main conclusions.

II. MODEL POTENTIAL AND COMPUTATIONAL METHOD

In the EAM,[11,16] the energy of a metallic system containing one species of atom is written as

$$E=\sum_i F_i(\overline{\rho_i})+\tfrac{1}{2}\sum_{\substack{i,j\\(i\neq j)}}\phi_{ij}(r_{ij}), \tag{1}$$

where $F_i(\overline{\rho_i})$ is the energy required to embed atom i into the background electron density at site i ($\overline{\rho_i}$), r_{ij} is the distance between atoms i and j, and $\phi_{ij}(r_{ij})$ is the core-core pair interaction between these atoms. The host electron density $\overline{\rho_i}$ is approximated by superimposing contributions by all the atoms surrounding atom i,

$$\overline{\rho_i}=\sum_{j(\neq i)}\rho_j(r_{ij}), \tag{2}$$

where $\rho_j(r_{ij})$ is the electron density of atom j at the position of the nucleus of atom i. If the atomic density function $\rho(r)$ and the pair interaction $\phi(r)$ are both known, the embedding energy can be uniquely defined by requiring that the energy given by Eq. (1) match the ''universal'' equation of state proposed by Rose *et al.*,[18] which gives the cohesive energy of the metal as a function of the lattice constant.

There are several EAM versions, which differ in the form of the functions involved and in the method used for their parametrization. In the version of Voter and Chen,[16] the atomic electron density is

$$\rho(r)=r^6(e^{-\beta r}+2^9e^{-2\beta r}), \tag{3}$$

β being an adjustable parameter, and the pairwise interaction is described by the Morse potential

$$\phi(r)=D_M\{1-\exp[-\alpha_M(r-R_M)]\}^2-D_M, \tag{4}$$

where D_M, R_M, and α_M, respectively, are the depth of the potential, the distance to the minimum, and a measure of the curvature at the minimum. The values of D_M, R_M, α_M, β, and the cutoff distance $r_{\rm cut}$ at which the functions $\phi(r)$ and $\rho(r)$ and their derivatives are forced to go smoothly to zero were determined by Voter and Chen for pure Ni and Al by minimizing the root-mean-square deviation between the calculated and experimental values of the three cubic elastic constants and the vacancy formation energy of each metal, and of the bond length and bond energy of the diatomic molecule [while requiring that $E(\text{fcc})<E(\text{hcp}), E(\text{bcc})$]. Including diatomic data in the parametrization procedure makes the potential more appropriate for describing the properties of small clusters, as we showed in Refs. 1 and 15.

The extension of Eq. (1) to a binary system is[16]

$$E=\sum_i F_{t_i}(\overline{\rho_i})+\tfrac{1}{2}\sum_{\substack{i,j\\(i\neq j)}}\phi_{t_it_j}(r_{ij}), \tag{5}$$

where the subscripts t_i and t_j indicate atom types and

$$\overline{\rho_i}=\sum_{j(\neq i)}\rho_{t_j}(r_{ij}). \tag{6}$$

Of the functions required by Eq. (5) for the binary system Ni-Al, $\phi_{\rm NiNi}$, $\phi_{\rm AlAl}$, $\rho_{\rm Ni}$, $\rho_{\rm Al}$, $F_{\rm Ni}$, and $F_{\rm Al}$ are known from previous work on the pure metals, leaving only $\phi_{\rm NiAl}$ to be determined. As in the case of the pure component, a Morse potential is used for this function. Equation (5) then involves seven adjustable parameters: D_M, R_M, α_M, $r_{\rm cut}$, $s_{\rm Ni}$, $g_{\rm Ni}$, and $g_{\rm Al}$, where the ''extra'' parameters $s_{\rm Ni}$, $g_{\rm Ni}$, and $g_{\rm Al}$ can be introduced because Eq. (5) is not, like Eq. (1), invariant when $\rho(r)$ is scaled or a linear term is added to $F(\overline{\rho})$ (see Ref. 16 for details). These seven parameters were optimized by Voter and Chen for a prediction of the experimental values of the Ni_3Al lattice constant, cohesive energy, elastic constants, vacancy formation energy, antiphase boundary energies, and superlattice intrinsic stacking fault energy, and of the lattice constant and cohesive energy of the $B2$ phase NiAl; it is Voter and Chen's values that were used in Eq. (5) to calculate, during our MD simulations, the forces experienced by the atoms in the clusters.

In the MD computations performed in this paper we used the velocity Verlet algorithm[19] with a time step of 10^{-3} ps, which guarantees conservation of the total cluster energy to within 0.01%. To obtain the lowest-energy structure of every cluster studied, an icosahedral configuration with zero total linear and angular momenta was heated to a high-temperature state close to evaporation. The system was then allowed to propagate over 2×10^6 steps, the atomic positions and velocities being recorded every 10^3 steps to obtain 2×10^3 uncorrelated configurations, to every one of which the steepest-descent method[20] was applied to obtain the corresponding local minimum of the potential-energy surface. The high energy of the 2×10^6-step trajectory ensures a thorough sampling of the configuration space. For each cluster studied, some 100–200 different local minima were located by this method.

For both the pure clusters Ni_{13}, Ni_{19}, Ni_{55}, Al_{13}, Al_{19}, and Al_{55} and the binary clusters $Ni_{n-x}Al_x$ ($n=13$, 19, and 55; $1\leqslant x\leqslant n-1$), the lowest of the minima found by the above thermal quenching method is in all cases icosahedral. However, due to the large number of possible locations of unlike atoms at the particle positions (especially with 55 atoms), reliable determination of the ground-state atomic configurations of the heteroclusters requires further exploration of the potential-energy surface. This was carried out as follows. Starting from the lowest-energy icosahedral configuration of the Ni_n cluster ($n=13$, 19, and 55), we constructed all the nonequivalent icosahedral $Ni_{n-1}Al$ clusters obtainable by replacing one Ni atom by one Al atom. To every one of these clusters, the steepest-descent method was applied to find icosahedral local minima for $Ni_{n-1}Al$. A similar procedure was applied to every one of these local minima (replacing one Ni atom by one Al atom) to locate icosahedral local minima of the clusters $Ni_{n-2}Al_2$; and soon for $Ni_{n-3}Al_3$, $Ni_{n-4}Al_4$, . . . ,$NiAl_{n-1}$. For each $Ni_{n-x}Al_x$, the ground-state configuration was taken to be that of the minimum with lowest energy. To check for consistency, the same procedure was then applied starting from Al_n ($n=13$, 19, and 55), and successively replacing Al atoms by Ni atoms until finally arriving at $Ni_{n-1}Al$.

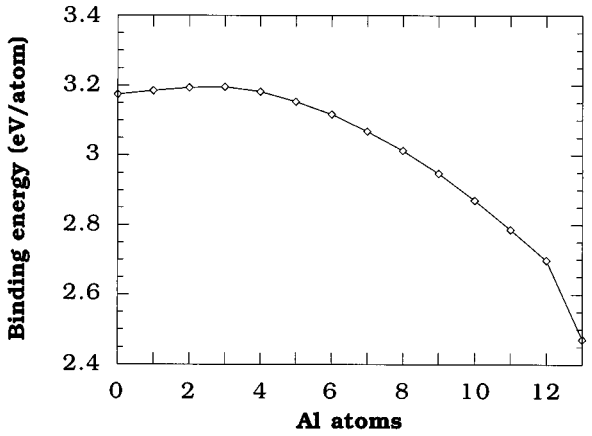

FIG. 1. Calculated binding energies of $Ni_{13-x}Al_x$ clusters as a function of Al concentration. Lines joining points are merely visual aids.

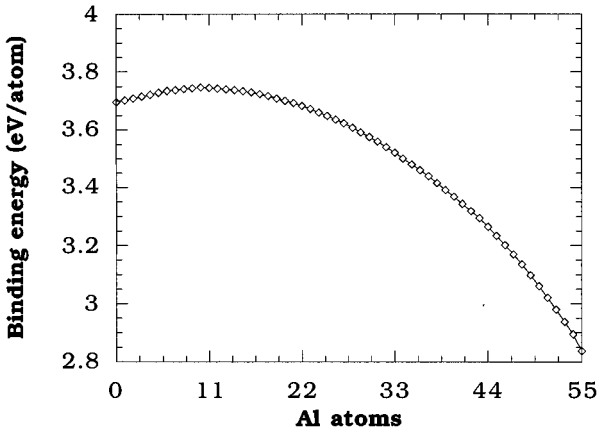

FIG. 3. Calculated binding energies of $Ni_{55-x}Al_x$ clusters as a function of Al concentration. Lines joining points are merely visual aids.

III. RESULTS AND DISCUSSION

Figures 1–3 show, for each of the clusters studied in this paper, the calculated binding energy of the ground-state configuration (i.e., the total minimum energy per atom, with the opposite sign). It should be noted that the binding energies of $Ni_{n-1}Al$ and $NiAl_{n-1}$ are greater than those of Ni_n and Al_n, respectively, for all three values of n. As indicated above, our EAM MD computations predict that the ground-state structures of all $Ni_{n-x}Al_x$ clusters ($n=13$, 19, and 55; $0 \leqslant x \leqslant n$) are icosahedral. Thus the mixing process does not modify the geometry of the pure Ni and Al clusters.

The prediction of icosahedral configurations for the one-component clusters Ni_{13}, Ni_{19}, and Ni_{55} agrees with the theoretical or simulational conclusions of a number of authors. Icosahedral geometry for Ni clusters containing up to $\approx$2300 atoms has been deduced by Cleveland and Landman[21] on the basis of an EAM with a different parametrization from that used in the present paper.[22] Icosahedral packing for Ni clusters in the size range $n=4$–23 has also been inferred by Stave and de Pristo[14] using a corrected effective-medium model. Our calculated binding energies for the icosahedral Ni_{13} and the double icosahedron Ni_{19}, 3.1742 and 3.3252 eV/atom, respectively, do not differ widely from the values 2.9100 and 3.0732 eV/atom obtained by Stave and de Pristo. More recently, Lathiotakis *et al.*[23] carried out TBM-based MD simulations to compare the structural stabilities of some fcc and icosahedral Ni clusters in the range $10<n\leqslant 55$, and found that although the two geometries are energetically competitive with each other, the icosahedral form is slightly the more stable on average. The binding energies obtained by Lathiotakis *et al.* for icosahedral Ni_{13} and the double icosahedron Ni_{19}, 3.16 and 3.33 eV/atom, respectively, are virtually the same as those afforded by our EAM MD calculations; however, our value of 3.6959 eV/atom for icosahedral Ni_{55} differs widely from that of Lathiotakis *et al.*, 4.27 eV/atom, which is much closer to the cohesive energy of the bulk fcc metal (4.45 eV/atom; Ref. 24). Experimental evidence of icosahedral geometry for Ni clusters has been inferred from adsorbate binding patterns.[25–28]

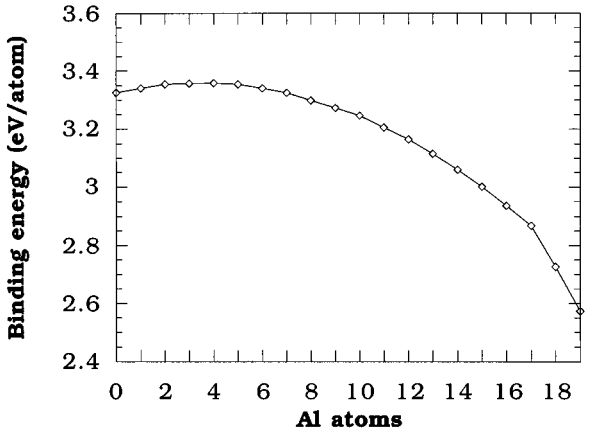

FIG. 2. Calculated binding energies of $Ni_{19-x}Al_x$ clusters as a function of Al concentration. Lines joining points are merely visual aids.

With regard to the prediction of icosahedral geometry for Al_{13}, Al_{19}, and Al_{55}, our results agree qualitatively with those arrived at by Yi *et al.*[29] using the original EAM version of Daw and Baskes,[30] although our calculated binding energies for these clusters, 2.4715, 2.5738, and 2.8367 eV/atom, respectively, are lower than the values 3.1231, 3.1684, and 3.2982 eV/atom obtained by Yi *et al.* These differences are not surprising: as we showed in Ref. 1, use of the properties of the diatomic molecule in parametrizing the embedding function and pair interaction, which is a main ingredient in the Voter and Chen EAM approach used in this paper, leads to lower binding energies than those obtained with other EAM versions.

As well as their EAM results, Yi *et al.*[29] also reported ground-state structures calculated for 13-, 19-, and 55-atom Al clusters by the Car-Parrinelo (CP) method.[31] These structures exhibit significant qualitative differences with respect to both their own EAM results and ours: according to the CP calculations, the icosahedron is more stable than the cuboctahedron for Al_{13} but is 1.9 eV less stable than the cuboctahedron for Al_{55}, while for Al_{19} the two structures have almost the same binding energy. These results, which are in keeping with density-functional calculations carried out by Cheng, Berry, and Whetten[32] and Pederson,[33] suggest that

TABLE I. Calculated binding energies E_c and E_i of ''closed-shell'' cuboctahedral and icosahedral Al_n clusters, in eV/atom.

n	E_c	E_i
13	2.4057	2.4715
55	2.8172	2.8367
147	2.9839	2.9897
309	3.0725	3.0730
561	3.1274	3.1254

the transition from an icosahedral structure to the fcc structure of bulk Al may occur at very low n, a striking phenomenon which is not reproduced by the EAM.

To determine the approximate cluster size at which the icosahedral-cuboctahedral transition does take place for Al according to the Voter and Chen EAM, we calculated the binding energies of ''closed-shell'' cuboctahedral and icosahedral Al_n clusters up to the first n for which the cuboctahedral binding energy exceeds that of the icosahedral structure. The results (Table I) show that crossover from one structure to the other occurs at $n=561$. By contrast, the same EAM approach gave the binding energies of the icosahedral and cuboctahedral Ni_{561} clusters as 4.1125 and 4.0946 eV/atom, respectively, which is consistent with previous calculations showing that, for Ni clusters, very large sizes are required for the appearance of a cuboctahedral structure.[21,34]

The cluster size at which the icosahedral-cuboctahedral transition occurs is determined by the balance between the surface cluster energy, which favors icosahedral symmetry, and the energy of the atoms inside the cluster, which favors the cuboctahedral arrangement. The difference in surface energy between these two geometries decreases as cluster size increases, and at some critical size becomes too small to outweigh the cuboctahedral preference of the internal atoms. The reason why the crossover between icosahedral and cuboctahedral structures occurs at a smaller size for Al than for Ni is a consequence of the fact that the energy contribution of distant atoms, relative to that of nearest neighbors, is larger for Al clusters (see Ref. 16 for details of Al-Al and Ni-Ni interactions). In fact, a reduction of about 9% in the cutoff distance of the Al-Al interaction makes the icosahedral Al_{561} cluster more stable than the corresponding cuboctahedral cluster. The influence of interactions with distant atoms on the critical size for structural transition in Cu, Ni, Pd, and Ag clusters has recently been studied by Montejano-Carrizales, Iñiguez, and Alonso[34] using FBD's version of the EAM.[11]

Before discussing in detail our predicted ground-state atomic configurations for $Ni_{n-x}Al_x$ ($n=13$, 19, and 55; $1\leqslant x\leqslant n-1$), it is worth mentioning that a feature of bulk Ni-Al is the large number of intermetallic compounds present in its phase diagram.[35] This suggests that ordering effects may also occur in small Ni-Al clusters. On the other hand, since Al has a lower surface energy than Ni (see, e.g., Ref. 36), it is equally to be expected that Al atoms may tend to occupy the cluster surface.[5,10,37]

Figure 4 shows the icosahedral ground-state atomic configurations of $Ni_{13-x}Al_x$ ($1\leqslant x\leqslant 12$). The icosahedra are slightly distorted due to the size difference between Ni and Al atoms. In $Ni_{12}Al$, the Al atom is located at the surface of the icosahedron. In principle, the strong tendency of the bulk alloy to form ordered compounds might suggest that the Al atom would prefer the cluster center, which would increase the number of Al-Ni bonds. However, if the larger Al atom were placed at the center of the icosahedron, the cluster would undergo a slight expansion, leading to energetically less favorable Ni-Ni bonds. Thus the atomic size mismatch prevents greater heterocoordination in $Ni_{12}Al$. The same phenomenon appears to occur at concentrations $x=2$–5, for all of which configurations with a larger number of Al-Ni bonds than those of the lowest-energy structures shown in Fig. 4 would be possible if the central atom were Al. It should be noted, however, that the lowest-energy structures of these clusters do maximize the number of Al-Ni surface bonds, so that segregation of Al at the cluster surface is accompanied by a kind of surface ordering. In the rest of the 13-atom clusters ($x=6$–12) the Al atoms are also located at the surface, but in these cases the ground-state atomic configurations maximize the total number of Al-Ni bonds, i.e., the Al segregation and ordering processes tend to produce the same effect. The predicted binding energy of icosahedral $NiAl_{12}$ (2.6976 eV/atom), in which a central Ni atom is surrounded by 12 Al atoms, is not too different from the estimate made by Gong and Kumar[17] using density-functional theory with the local-spin-density approximation (2.9699 eV/atom). Figure 1 shows that among all the $Ni_{13-x}Al_x$ clusters, binding energy peaks at $x=3$, the largest value of x for which the corresponding cluster lacks any Al-Al bond (see Fig. 4); note that the attraction of Al for Al is weaker than that of Ni for Ni or Ni for Al, as is shown by the energies of the diatomic bonds.[16]

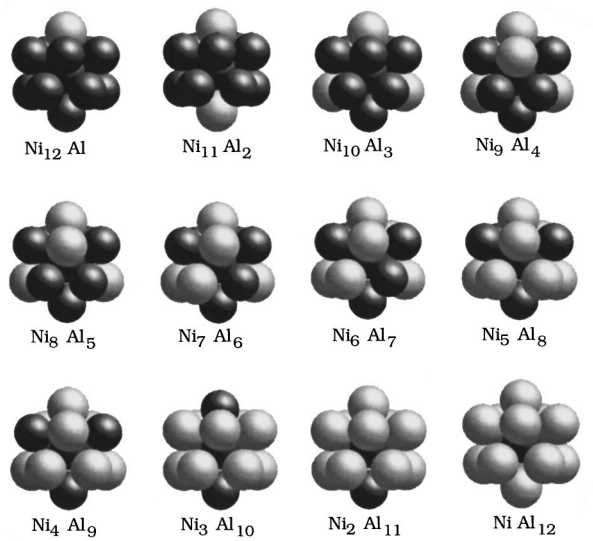

FIG. 4. Ground-state atomic configurations of bimetallic $Ni_{13-x}Al_x$ clusters. Light gray and dark gray spheres represent Al and Ni atoms, respectively.

The bimetallic $Ni_{19-x}Al_x$ clusters have double icosahedral structures, which can be thought of either as two interpenetrating 13-atom icosahedra, or as two pentagonal bipyramids laid end to end with five atoms forming a central belt around the resulting ''waist.'' The calculated ground-state atomic configurations of these clusters are shown in Fig. 5. The Al atoms are always located at the cluster surface (except, of course, in the case of $NiAl_{18}$, in which one Al atom

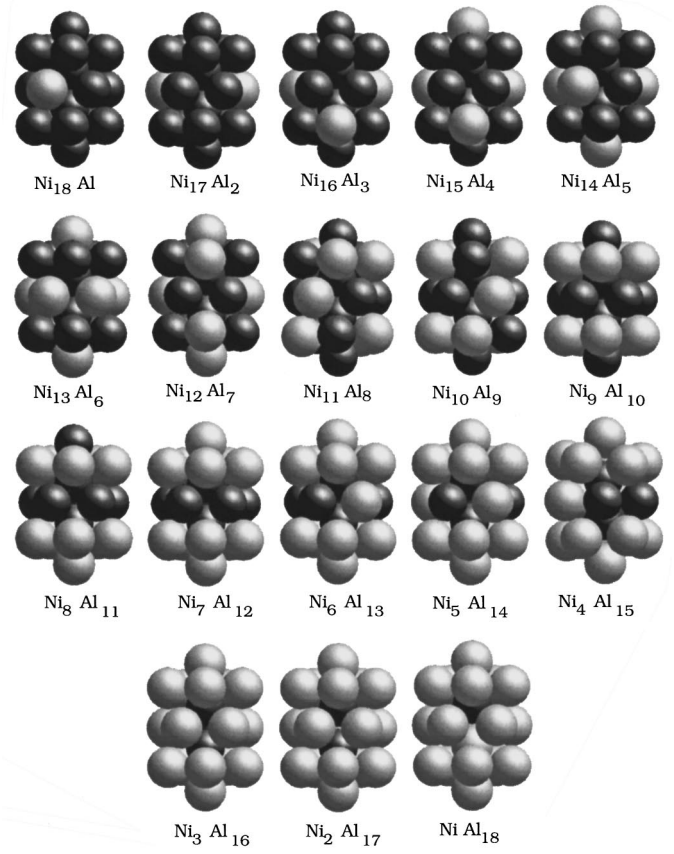

FIG. 5. Ground-state atomic configurations of bimetallic $Ni_{19-x}Al_x$ clusters. Light gray and dark gray spheres represent Al and Ni atoms, respectively.

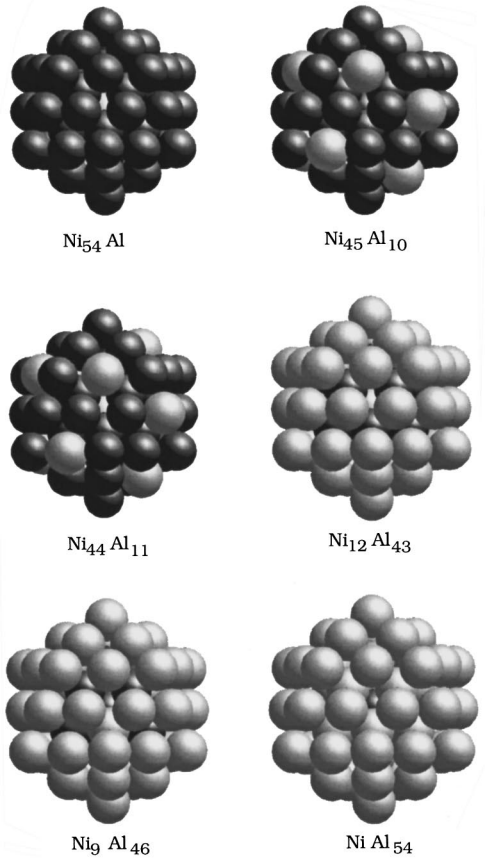

FIG. 6. Ground-state atomic configurations of some bimetallic $N_{55-x}Al_x$ clusters. Light gray and dark gray spheres represent Al and Ni atoms, respectively.

must occupy one of the two central sites). For $x=1$ the number of Al-Ni bonds would be maximum if the Al atom were located in the core of the cluster, but, as in the case of $Ni_{12}Al$, this is prevented by size mismatch effects. Note, however, that the position of the Al atom, in the central belt, maximizes the number of Al-Ni surface bonds. This maximization of surface heterocoordination recurs throughout the range $x=2$–10. For large Al concentrations ($x=16$, 17, and 18), the ground-state atomic configurations maximize the total number of Al-Ni bonds, so that in these cases there is no conflict between ordering and surface Al segregation. Among all the $Ni_{19-x}Al_x$ clusters, binding energy peaks for $x=4$ (Fig. 2), the largest value of x for which the corresponding cluster lacks any Al-Al bond (see Fig. 5).

The ground-state structures of the bimetallic $Ni_{55-x}Al_x$ clusters consist of one central atom and two concentric shells, one with 12 atoms and the other with 42. Of the 42 atoms in the surface shell, 12 are at vertex positions and the rest at edge sites. Figure 6 shows an illustrative sample. In $Ni_{54}Al$ the Al atom lies at the 12-coordinate central site, maximizing the number of Al-Ni bonds (although this distribution is almost equienergetic with a configuration in which the Al atom occupies an edge site at the cluster surface). Thus unlike $Ni_{12}Al$ and $Ni_{18}Al$, the larger $Ni_{54}Al$ cluster is not dominated, as regards the position of the Al atom, by atomic size mismatch effects (the presence of the central Al hardly modifies the positions of the surface-shell Ni atoms with respect to those they occupy in Ni_{55}), and ordering predominates over the tendency for Al to segregate at the surface. For $x=2$–10, however, all the Al atoms of the $Ni_{55-x}Al_x$ clusters are at edge sites on the surface. In these clusters, Al surface segregation is accompanied by surface ordering, since the number of surface Al-Ni bonds is maximized by placing the Al atoms at edge sites (which are eight-coordinate, whereas vertex sites are only six-coordinate). $Ni_{45}Al_{10}$ (Fig. 6) has the largest binding energy of all $Ni_{55-x}Al_x$ clusters (see Fig. 3), and the highest Al concentration of all bimetallic $Ni_{55-x}Al_x$ clusters with no central Al and no Al-Al bond. If a Ni atom at the surface of $Ni_{45}Al_{10}$ were replaced by an Al atom to form $Ni_{44}Al_{11}$, at least one Al-Al bond would be formed. To avoid this, the ground-state atomic configuration of $Ni_{44}Al_{11}$ is the same as that of $Ni_{45}Al_{10}$, save that the cluster center is now occupied by an Al atom (see Fig. 6). Except in $Ni_{42}Al_{13}$, in which all the Al atoms are at the surface, this central Al is retained throughout the range $x=11$–43, the remaining Al atoms all lying at the surface; and the exceptional configuration of $Ni_{42}Al_{13}$ is almost equienergetic with a configuration in which there is an Al atom at the cluster center. In $Ni_{12}Al_{43}$ the inner shell is composed entirely of the 12 Ni atoms, each of which has seven Al neighbors (the central atom and six surface atoms); while the surface shell is composed entirely of Al atoms (Fig. 6). Thus surface segregation of Al atoms coincides with ordering in this cluster. The lowest-energy atomic configurations of $Ni_{11}Al_{44}$ and $Ni_{10}Al_{45}$ are similar to that of $Ni_{12}Al_{43}$, the extra Al atoms replacing Ni atoms in the inner shell. For $x=46$–54, however, although the surface is composed of Al

atoms, there is now a Ni atom at the cluster center (Fig. 6, Ni_9Al_{46} and $NiAl_{54}$). In $NiAl_{54}$, the Ni atom occupies the 12-coordinate central site and is surrounded by Al atoms filling the inner and surface shells, so that Al surface segregation and ordering effects coincide.

IV. SUMMARY AND CONCLUSIONS

In this work we performed MD simulations to study the ground-state atomic configurations of $Ni_{13-x}Al_x$, $Ni_{19-x}Al_x$, and $Ni_{55-x}Al_x$ clusters for all concentrations x. The model used to describe the interactions between the atoms in the clusters was the EAM as parametrized by Voter and Chen,[16] which incorporates the necessary many-body character of metallic cohesion. The main difference between this model and other EAM versions is that it includes diatomic data in optimizing the embedding functions and pair interactions, thus providing a more appropriate framework for studying the properties of small metal clusters.

Our EAM MD calculations predict that the lowest-energy structures of pure Ni_n and Al_n clusters and bimetallic $Ni_{n-x}Al_x$ clusters ($1 \leqslant x \leqslant n-1$) are icosahedral for $n=13$, 19, and 55. Thus mixing Ni and Al does not modify the geometry of the 13-, 19-, and 55-atom clusters, which are icosahedral for all concentrations. The predicted icosahedral structures of Ni_{13}, Ni_{19}, Ni_{55}, Al_{13}, and Al_{19} are in keeping with both the experimental and theoretical findings of other authors.[14,21,23,25–29,32,33] However, the computed icosahedral geometry for pure Al_{55} is at variance with the CP results of Yi *et al.*[29] and with the density-functional calculations of Cheng, Berry, and Whetten[32] and Pederson,[33] which predict that the cuboctahedral configuration is slightly more stable than the icosahedral configuration for Al_{55}. In spite of these authors' results, which suggest that the transition from the icosahedral to the bulk structure may occur very early in the growth of Al clusters, there are reasons to believe that $Ni_{55-x}Al_x$ heteroclusters, like $Ni_{13-x}Al_x$ and $Ni_{19-x}Al_x$, are probably icosahedral, as predicted in the present paper. Recent MD simulations carried out by López, Marcos, and Alonso[7] on $Cu_{14-x}Au_x$ clusters using a tight-binding potential show that although Au_{14} has a nonicosahedral structure, bimetallic $Cu_{14-x}Au_x$ clusters prefer the icosahedral packing of Cu_{14} for all x. This means that replacement of just one Au atom by a Cu atom in the nonicosahedral Au_{14} cluster suffices to make its lowest-energy structure icosahedral.

The computed ground-state atomic configurations of the bimetallic $Ni_{n-x}Al_x$ clusters ($n=13$, 19, and 55) show that there is a general tendency for Al to segregate at the cluster surfaces. This result is in consonance with the common finding of recent studies that bimetallic clusters exhibit surface segregation of the atom with smaller surface energy.[5,10,37] Our results therefore support the reliability of the Voter and Chen EAM for describing the properties of this kind of heterocluster.

There are also ordering effects in the bimetallic $Ni_{n-x}Al_x$ clusters, as is to be expected given the strong compound-forming tendency of bulk Ni-Al. These two effects, ordering and surface Al segregation, can coexist. When the two effects conflict, surface Al segregation generally prevails, but even then it coexists with a kind of surface ordering. In this respect the behavior of the bimetallic Ni-Al clusters is similar to that of Cu-Pd clusters, which have been studied by Montejano-Carrizales, Iñiguez, and Alonso[10] for several sizes and concentrations using the EAM version of Foiles, Baskes, and Daw,[11] and assuming ideal structures with fixed interatomic distances.

The behavior of the large cluster $Ni_{54}Al$ differs from that of the smaller clusters with single Al ''impurities,'' $Ni_{12}Al$ and $Ni_{18}Al$. Whereas in the latter the Al atom is at the cluster surface, showing predomination of surface Al segregation over ordering, in $Ni_{54}Al$ the Al atom is located at the 12-coordinate central site, showing ordering to be the dominant effect, in closer resemblance with the bulk behavior. These differences can be attributed to size mismatch effects, which are less pronounced for large cluster sizes. Experiments confirming these predictions would be of interest.

ACKNOWLEDGMENTS

This work was supported by the DGICYT, Spain (Project No. PB92-0645-C03-03), and the Xunta de Galicia (Project No. XUGA20602B92).

[1] C. Rey, L. J. Gallego, J. García-Rodeja, J. A. Alonso, and M. P. Iñiguez, Phys. Rev. B **48**, 8253 (1993).
[2] A. S. Clarke, R. Kapral, B. Moore, G. N. Patey, and X.-G. Wu, Phys. Rev. Lett. **70**, 3283 (1993).
[3] A. S. Clarke, R. Kapral, and G. N. Patey, J. Chem. Phys. **101**, 2432 (1994).
[4] C. Rey and L. J. Gallego, Phys. Rev. B **51**, 13 691 (1995).
[5] L. Yang, T. J. Raeker, and A. E. DePristo, Surf. Sci. **290**, 195 (1993).
[6] G. E. López and D. L. Freeman, J. Chem. Phys. **98**, 1428 (1993).
[7] M. J. López, P. A. Marcos, and J. A. Alonso, J. Chem. Phys. **104**, 1056 (1996).
[8] J. H. Sinfelt, *Bimetallic Catalysts: Discoveries, Concepts and Applications* (Wiley, New York, 1983).
[9] K. C. Taylor, *Automobile Catalytic Converters* (Springer, New York, 1984).
[10] J. M. Montejano-Carrizales, M. P. Iñiguez, and J. A. Alonso, Phys. Rev. B **49**, 16 649 (1994).
[11] S. M. Foiles, M. I. Baskes, and M. S. Daw, Phys. Rev. B **33**, 7983 (1986).
[12] F. Ducastelle, J. Phys. (Paris) **31**, 1055 (1970).
[13] C. Massobrio, V. Pontikis, and G. Martin, Phys. Rev. B **41**, 10 486 (1990).
[14] M. S. Stave and A. E. DePristo, J. Chem. Phys. **97**, 3386 (1992).
[15] J. García-Rodeja, C. Rey, L. J. Gallego, and J. A. Alonso, Phys. Rev. B **49**, 8495 (1994).
[16] A. F. Voter and S. P. Chen, in *Characterization of Defects in Materials*, edited by R. W. Siegal, J. R. Weertman, and R. Sinclair, MRS Symposia Proceedings No. 82 (Materials Research Society, Pittsburgh, 1987), p. 175.
[17] X. G. Gong and V. Kumar, Phys. Rev. B **50**, 17 701 (1994).
[18] J. H. Rose, J. R. Smith, F. Guinea, and J. Ferrante, Phys. Rev. B **29**, 2963 (1984).

[19] W. C. Swope, H. C. Andersen, P. H. Berens, and K. R. Wilson, J. Chem. Phys. **76**, 637 (1982).
[20] F. H. Stillinger and T. A. Weber, Phys. Rev. A **25**, 978 (1982).
[21] Ch. L. Cleveland and U. Landman, J. Chem. Phys. **94**, 7376 (1991).
[22] J. B. Adams, S. M. Foiles, and W. G. Wolfer, J. Mater. Res. **4**, 102 (1989).
[23] N. N. Lathiotakis, A. N. Andriotis, M. Menon, and J. Connolly, Europhys. Lett. **29**, 135 (1995).
[24] *Smithells Metals Reference Book*, 7th ed., edited by E. A. Brandes and G. B. Brook (Butterworth-Heinemann, London, 1992), p. 8-2.
[25] E. K. Parks, B. J. Winter, T. D. Klots, and S. J. Riley, J. Chem. Phys. **94**, 1882 (1991).
[26] E. K. Parks, L. Zhu, J. Ho, and S. J. Riley, J. Chem. Phys. **100**, 7206 (1994).
[27] E. K. Parks, L. Zhu, J. Ho, and S. J. Riley, J. Chem. Phys. **102**, 7377 (1995).
[28] E. K. Parks and S. J. Riley, Z. Phys. D **33**, 59 (1995).
[29] J.-Y. Yi, D. J. Oh, J. Bernholc, and R. Car, Chem. Phys. Lett. **174**, 461 (1990).
[30] M. S. Daw and M. I. Baskes, Phys. Rev. B **29**, 6443 (1984).
[31] R. Car and M. Parrinello, Phys. Rev. Lett. **55**, 2471 (1985).
[32] H.-P. Cheng, R. S. Berry, and R. L. Whetten, Phys. Rev. B **43**, 10 647 (1991).
[33] M. R. Pederson, in *Physics and Chemistry of Finite Systems: From Clusters to Crystals*, Vol. 374 of *NATO Advanced Science Institutes Series, Series C: Mathematical and Physical Sciences*, edited by P. Jena, S. N. Khanna, and B. K. Rao (Kluwer Academic, Dordrecht, 1992), p. 861.
[34] J. M. Montejano-Carrizales, M. P. Iñiguez, and J. A. Alonso, J. Cluster Sci. **5**, 287 (1994).
[35] R. Hultgren, P. D. Desai, D. T. Hawkins, M. Gleiser, and K. K. Kelley, *Selected Values of the Thermodynamic Properties of Binary Alloys* (American Society for Metals, Metals Park, OH, 1973).
[36] J. A. Alonso and N. H. March, *Electrons in Metals and Alloys* (Academic, New York, 1989).
[37] L. Zhu and A. E. DePristo, J. Chem. Phys. **102**, 5342 (1995).